

DEUTSCHES ELEKTRONEN-SYNCHROTRON **DESY**

DESY 87-027  
April 1987



HADRON-, ELECTRON- AND MUON-RESPONSE  
OF A URANIUM-SCINTILLATOR CALORIMETER

by

M.G. Catanesi

*Università di Bari and INFN, Bari*

G. Crosetti, M. Fidecaro

*CERN, Geneva*

E. Bernardi, R. Klanner, D. Lüke, R. Walczak

*Deutsches Elektronen-Synchrotron DESY, Hamburg*

M. Gennis, R. Langkau, W. Scobel

*I. Institut f. Experimentalphysik, Universität Hamburg*

J. Krüger, J.H. Peters, H. Spitzer

*II. Institut f. Experimentalphysik, Universität Hamburg*

M.J. Esten

*University College, London*

M. de Vincenzi, A. Frenkel, E. Lamanna, G. Marini, G. Martellotti,

A. Nigro, G. Penso, P. Pistilli, A. Sciubba

*Università di Roma "La Sapienza" and INFN, Rome*

ISSN 0418-9833

**NOTKESTRASSE 85 · 2 HAMBURG 52**

**DESY behält sich alle Rechte für den Fall der Schutzrechtserteilung und für die wirtschaftliche Verwertung der in diesem Bericht enthaltenen Informationen vor.**

**DESY reserves all rights for commercial use of information included in this report, especially in case of filing application for or grant of patents.**

**To be sure that your preprints are promptly included in the  
HIGH ENERGY PHYSICS INDEX ,  
send them to the following address ( if possible by air mail ) :**

**DESY  
Bibliothek  
Notkestrasse 85  
2 Hamburg 52  
Germany**

## Hadron-, Electron- and Muon-Response of a Uranium-Scintillator Calorimeter

M.G. Catanesi

*Università di Bari and INFN, Bari, Italy*

G. Crosetti<sup>1</sup>, M. Fidecaro

*CERN, Geneva, Switzerland*

E. Bernardi, R. Klanner, D. Lüke, R. Walczak<sup>2</sup>

*DESY, Hamburg, Fed. Rep. Germany*

M. Gennis, R. Langkau, W. Scobel

*I. Institut für Experimentalphysik, Universität Hamburg, Fed. Rep. Germany*

J. Krüger, J.H. Peters, H. Spitzer

*II. Institut für Experimentalphysik, Universität Hamburg, Fed. Rep. Germany*

M.J. Esten

*University College, London, United Kingdom*

M. De Vincenzi, A. Frenkel, E. Lamanna, G. Marini, G. Martellotti, A. Nigro,

G. Penso, P. Pistilli, A. Sciubba

*Università di Roma "La Sapienza" and INFN, Rome, Italy*

- Members of WA-78, H1 and ZEUS Collaborations -

*(Submitted to Nuclear Instruments and Methods)*

### Abstract

A hadron calorimeter comprising 10 mm depleted uranium plates and 5 mm plastic scintillator was exposed to electrons, hadrons and muons in the energy range 5 to 210 GeV. The measured ratios of sampling fractions are 0.8 for " $e/\pi$ " and 0.6 for " $e/mip$ ". The addition of a fine grained electromagnetic calorimeter with 1.6 mm depleted uranium plates and 4 mm plastic scintillator in front of the hadron calorimeter leads to a slightly worse hadronic energy resolution. Results on the longitudinal shower development and energy containment for hadron showers are given.

<sup>1</sup>Now at INFN, Genoa, Italy

<sup>2</sup>On leave from Warsaw University, Poland

## 1 Introduction

Experimentation at future high energy colliders requires the development of hadron calorimeters with fine granularity and excellent energy resolution. This work is part of a systematic program investigating the energy resolution of sampling calorimeters using depleted uranium as absorber and plastic scintillator as detector material. Such a calorimeter is proposed by the ZEUS collaboration at the HERA electron proton storage ring [1].

This paper presents results obtained in the energy range from 5 to 210 GeV with the WA-78 calorimeter (10 mm depleted uranium and 5 mm plastic scintillator) alone, and together with a fine grained electromagnetic calorimeter (1.57 mm uranium and 4 mm plastic scintillator) in front. It is an extension of the previous work of the WA-78 collaboration [2,3], which has investigated different uranium thicknesses and uranium-iron combinations as absorbers in the energy range 135 to 350 GeV.

In this paper we compare the response of the calorimeter to muons, hadrons and electrons in a wide energy range. The choice of the material thicknesses (10 mm uranium and 5 mm plastic scintillator), although not optimized for energy resolution, is of particular interest for the understanding of compensation in calorimetry. With these parameters, the slow neutron component of hadronic showers, which can be used to optimize the hadronic energy resolution by equalizing electromagnetic and hadronic response, is detected with particularly high efficiency. As a result the relative response of electrons to hadrons - significantly bigger than 1 in noncompensating calorimeters - is 0.80. Its value as a function of energy and signal integration time is investigated in this paper. Using the muon response to normalize the scale of deposited energy, the sampling fraction of electromagnetic showers is determined, and compared to the sampling fraction of minimum ionizing particles.

Finally, longitudinal shower distributions are presented as a function of energy, and criteria for shower containment are discussed.

## 2 Experimental Set-Up

A schematic view of the experimental set-up is shown in Fig. 1. It consists of beam defining counters, a threshold Čerenkov counter for particle identification, an electromagnetic and a hadronic calorimeter. Details of the layer structure of the calorimeters are given in Tab. 1.

Incoming beam particles are defined by the following coincidence of signals from scintillation counters:

$$\text{BEAM} = B1 \cdot B2 \cdot \overline{H1} \cdot \overline{H2} \cdot \overline{A}$$

The scintillator array F (5 vertical elements of 1 cm width each) is used to measure the horizontal beam position.

The hadronic calorimeter ("HAD" in the figure), readout electronics and calibration procedures have already been described in [2], and we only repeat the most significant features. Longitudinally it consists of two sections. The upstream "Uranium Part" is made of 48 elements (absorber and scintillator) grouped in 12 modules, each viewed by one photomultiplier. This part was designed to permit easy exchange of absorbers, and has previously been used with iron and uranium plates of different thicknesses. In the present work uranium layers ( $60 \times 60 \times 1\text{cm}^3$ ) enclosed in 1 mm steel, and 5 mm scintillator (NE 110) have been used. The downstream "Iron Part" consists of 52 elements with 2.5 cm iron plates as absorber and

0.5 cm plastic scintillator, grouped in 13 modules. Optical fibres couple the scintillator to low gain photomultipliers (THORN-EMI D254A), followed by LeCroy VV100BTB amplifiers. The signals are split and recorded by LeCroy FERA 4300 ADCs with 45 ns and 75 ns gate length. The gain of the photomultipliers was monitored using light emitting diodes.

The calibration of the individual photomultipliers was done by the method described in [2]: the average longitudinal shower development for hadrons is independent of the starting point of the shower. This results in an over-determined system of linear equations relating the calibration constants to the measured average pulse heights when data samples of showers, starting in the different modules, are selected. Analysing the data at various beam momenta indicates that the calibration constants thus determined have a maximum uncertainty of  $\pm 4\%$  for the first module and  $\pm 3\%$  for the other modules. The calibration has been checked using muons of various momenta. The stability of the system was sufficient that the entire data could be analysed with a single set of calibration constants.

The electromagnetic calorimeter "EM" [4,12] is made of six identical modules: each one consists of a mechanical frame (4 mm Al) supporting light guides and photomultipliers, 9 scintillator plates (SCSN-38.  $31.2 \times 31.8 \times 0.4\text{cm}^3$ ), interspaced with 8 depleted uranium plates ( $30 \times 30 \times 0.157\text{cm}^3$ ) enclosed in 0.5 mm steel. The light from the scintillator is collected by wavelength shifter plates (3 mm plexiglass doped with Y-7) on both sides, which transport the light to the photomultipliers (Philips XP-2011B). Again the signals are split and recorded by LeCroy FERA ADCs. Light emitting diodes are used to monitor the stability of the gain of the photomultipliers.

Each module can be moved out of the beam line independently. In this way it is easy to change from running conditions with the electromagnetic calorimeter in or out of the beam. For calibration the six modules are moved one by one out of the beam, and the average pulse height is normalized when the particular module is the first module in the beam. The estimated calibration uncertainty is about 1%. This was checked with interacting hadrons, using the same method as for the hadron calorimeter. The relative calibration of the two calorimeters is discussed in section 3.3.

The experiment used the H3 beam line of the CERN-SPS. In order to reach low momenta, without interfering with other beam lines in the hall, a secondary target was introduced in the downstream part of the H3-beam. Behind the target only a small amount of magnetic bending was left. This resulted in a poor momentum resolution, which has been estimated by beam optics calculations including multiple scattering to be approximately:

$$\left(\frac{\sigma_p}{p}\right)^2 = (0.07)^2 + \left(\frac{0.14}{\sqrt{p}}\right)^2 \quad (1)$$

For particle identification an 11 m long threshold Čerenkov counter  $\hat{C}$  (Fig. 1) filled with He was used. Its gas pressure was adjusted to obtain the best electron-hadron separation at the different momenta. The particle content of the beam was measured using the Čerenkov counter and the longitudinal energy distribution in the calorimeter. The results are given in Tab. 2.

### 3 Experimental Results

Data have been taken in the two different configurations:

1. hadronic calorimeter (HAD)
2. electromagnetic calorimeter followed by the hadronic calorimeter (EM + HAD)

The beam momenta were 5, 10, 20, 30 and 40 GeV/c. Data were also taken at 135 and 210 GeV/c to compare with previous results [2].

#### 3.1 Response to Hadrons, Electrons and Muons

As an example, Fig. 2 shows the pulse height measured for configuration 1 (HAD only) at 30 GeV for hadrons, electrons and muons. The responses for electrons and hadrons are fitted by Gaussian functions; for muons a Landau curve convoluted by a Gaussian is used. Fig. 3 shows the response for electrons and hadrons of different momenta. To determine mean values and standard deviations we performed a Gaussian fit over  $\pm 3$  standard deviations. The resulting values of standard deviations and mean values for the configurations HAD and EM + HAD are given in Tab. 3 in units of ADC-channels. For the hadronic calorimeter alone the ratio of electron to hadron response ( $\epsilon/\pi$ ) is also given. The value is about 0.8. It should be noted that the transverse size of the calorimeter is not sufficient to fully contain hadronic showers. From data of the ZEUS-test-calorimeter [5], we estimate a transverse leakage of about 5 %, mainly due to slow neutrons, which leads to an increased, observed  $\epsilon/\pi$ -ratio.

Fig. 4 displays  $\epsilon/\pi$ -ratios for different hadron calorimeters using uranium as absorber and scintillator as detector. It should be noted that the data are measured  $\epsilon/\pi$ -ratios, not corrected for experimental effects like inhomogeneities of readout or leakage. Whereas for calorimeters with Fe or Pb as absorbers  $\epsilon/\pi$  is greater than 1 [9,10], uranium scintillator calorimeters can achieve  $\epsilon/\pi = 1$  (compensating) or even  $\epsilon/\pi < 1$  (overcompensating) as in the present calorimeter, depending on the choice of absorber and scintillator thickness.

At high energies, compensating calorimeters achieve the best energy resolution, as their response does not depend on the fluctuations between the electromagnetic and the hadronic components of hadron showers. It is generally agreed that the increased response for hadron showers in uranium calorimeters is dominantly due to slow neutrons from spallation and fission, which scatter elastically off the free protons in the plastic scintillator [10,11]. In contrast to the prompt signal from the relativistic particles in the shower, the neutron signal is delayed since the neutrons deposit their energy in several successive interactions. With increased integration time, more and more of the neutron signal will be recorded and the  $\epsilon/\pi$ -ratio will decrease. Fig. 5 shows the dependence of the  $\epsilon/\pi$ -ratio on the gating time of the ADC which shows the expected behaviour<sup>1</sup>.

Tab. 3 also gives the energy resolution  $\sigma_E(\epsilon)/E$  for electrons and  $\sigma_E(\pi)/E$  for hadrons. As discussed in section 2, this has a large contribution from the momentum spread of the beam. The electromagnetic calorimeter EM equipped with 3 mm lead plates has achieved an energy resolution of  $10.2\%/\sqrt{E}$  in the 1 to 5 GeV energy range at tests done at DESY [4,12]. The measured energy resolution for hadrons of the hadronic calorimeter HAD can be parametrized

<sup>1</sup>In the measurement, the start of the gate preceded the photomultiplier pulse by about 15 ns, which reduces the effective gate length.

by:

$$\left(\frac{\sigma_E(\pi)}{E}\right)^2 = (0.07)^2 + \left(\frac{0.51}{\sqrt{E}}\right)^2 \quad (2)$$

This includes the momentum uncertainty of the beam (1), which gives a significant contribution particularly at high energies.

#### 3.2 Electromagnetic Sampling Fraction

The simultaneous measurement of muons and electrons allows a determination of "e", defined as the fraction of incident energy measured in the active medium of the calorimeter for electromagnetic showers. Fig. 6 displays the muon spectrum at 30 GeV in the electromagnetic calorimeter. In table 3 we give the average response for muons of the different energies. To estimate the mean energy  $\Delta E(\mu)|_{SC1}$  in MeV detected in the scintillator for muons traversing the calorimeter we use two methods which we expect to give an upper and lower estimate of the correct value. We prefer to use the mean value of the deposited energy  $\Delta E(\mu)$ , which is proportional to the absorber thickness (not the case for the most probable value).

- Method 1 assumes that none of the energy lost by the muons in the absorber is transferred to the scintillator and vice versa. The values for the energy loss including ionization (Ion), bremsstrahlung (Brems) and pair production (Pair) are taken from [13] by interpolation and are listed in table 4. We do not take into account hadronic interactions of muons, as these events are removed by cuts in the analysis:

$$\Delta E(\mu)|_{SC1}^{meth.1} = \left( \frac{dE}{dx}(\mu) \Big|_{SC1}^{Ion} + \frac{dE}{dx}(\mu) \Big|_{SC1}^{Brems} + \frac{dE}{dx}(\mu) \Big|_{SC1}^{Pair} \right) \cdot \Delta x_{SC1} \quad (3)$$

- method 2 assumes that the energy seen in the scintillator is the sum of ionization loss in the scintillator plus the energy lost by bremsstrahlung and pair production in the entire calorimeter (absorber plus detector) multiplied by "e", the sampling fraction of electromagnetic showers:

$$\Delta E(\mu)|_{SC1}^{meth.2} = \frac{dE}{dx}(\mu) \Big|_{SC1}^{ion} \cdot \Delta x_{SC1} + "e" \cdot \left\{ \Delta E(\mu)|_{CAL}^{Brems} + \Delta E(\mu)|_{CAL}^{Pair} \right\} \quad (4)$$

with:

$$\Delta E(\mu)_{CAL}^i = \frac{dE}{dx}(\mu)_{SCI}^i \cdot \Delta x_{SCI} + \sum_{ABS} \frac{dE}{dx}(\mu)_{ABS}^i \cdot \Delta x_{ABS} \quad (5)$$

where we sum over the different types of absorber materials in the calorimeter.

Given the measured pulse heights  $PH(e)$  and  $PH(\mu)$  for electrons and muons and the calculated energy loss  $\Delta E(\mu)_{SCI}$  using the values from [13], the sampling fraction is

- method 1:

$$r_e = \frac{\Delta E(\mu)_{SCI}^{meth.1}}{PH(\mu)} \cdot \frac{PH(e)}{E} \quad (6)$$

- method 2:

$$r_e = \frac{\Delta E(\mu)_{SCI}^{Ion}}{PH(\mu) \cdot \left\{ 1 - \left( \Delta E(\mu)_{CAL}^{Brem} + \Delta E(\mu)_{CAL}^{Pair} \right) \cdot \frac{PH(e)}{E \cdot PH(\mu)} \right\}} \cdot \frac{PH(e)}{E} \quad (7)$$

The results are given in Tab. 4. We estimate a systematic error of 7% due to uncertainties in calibration constants (2%), absorber- and scintillator thickness (4% for the EM- and 1% for the HAD- calorimeter), beam energy (2%) and non-linearity of the ADCs (5%).

At an energy of  $E=10.14$  GeV the electron sampling fraction  $r_e$  has been calculated with EGS4 shower simulations for the HAD-calorimeter, yielding  $r_e = 2.28$  %. The cut-off energies chosen are 10 keV for electrons and 1 keV for photons. In addition, the fractional energy loss per step was set to 0.1 % for low-Z and 0.5 % for high-Z absorbers.

For the comparison of calorimeters with different layer structures,  $r_e$  is often normalized to the sampling fraction "mip" of a hypothetical minimum ionizing particle with an energy-loss at the minimum of the ionization curve throughout the calorimeter. The result and the constants needed for its calculation are given in Tab. 5. For both calorimeters  $r_e/mip$  is smaller than 1. The reasons have been explained in [10,11]. The different electromagnetic processes have very different Z-dependences (e.g.  $Z^1$  for ionization loss,  $Z^2$  for pair production and  $Z^{-5}$  for the photo effect). In particular most of the low energy electrons from the photo effect get produced in the high-Z absorber and due to their small range they also deposit practically all their energy there. Thus the low energy component of electromagnetic showers gets only poorly sampled in the scintillator. The difference in the measured  $r_e/mip$  ratios of the two different calorimeters is expected too. The main effect is not due to the thickness of the absorber plates but due to the relatively small fraction of uranium absorber in the EM calorimeter, resulting in a reduced effective Z.

### 3.3 Combined Electromagnetic and Hadronic Calorimeter

To study questions related to the performance of a calorimeter consisting of two parts with different sampling, data have been taken with the fine-grained electromagnetic calorimeter (EM) in front of the coarse hadronic calorimeter (HAD). Results are only given for the data at 30 GeV/c, the results at the other energies being similar. For the calibration within the two calorimeters, the constants of section 2 have been taken. The pulse heights from the electromagnetic and the hadronic calorimeter have been combined according to:

$$PH_{TOT} = PH_{EM} + \alpha \cdot PH_{HAD}. \quad (8)$$

Fig. 7 shows the energy resolution for electrons and hadrons as a function of the relative calibration constant  $\alpha$ . The energy resolution for electrons is constant, as most of the energy is contained in the electromagnetic section. The resolution for hadrons is best for  $\alpha = 2.25$  with a value of 12.5%. The corresponding energy resolution of the hadronic calorimeter alone is 12.1%. The value  $\alpha = 3.45$ , which gives the same pulse height for electrons in both calorimeters, yields 17% resolution. Normalizing to equal ratio of muon signal over "mip"-sampling fraction gives  $\alpha = 2.72$  and 13.5% resolution. Another calibration method frequently used requires that the total pulse height be independent of the energy sharing in the two calorimeters. This gives  $\alpha = 2.17$  and 12.5% resolution.

We conclude therefore, that there is quite some arbitrariness in the relative calibration if a calorimeter consists of two parts with different sampling resulting in different resolution values – all of them, however, being worse than the resolution of the coarse calorimeter alone. This result agrees with expectations, as the  $r_e/\pi$  ratios of the two calorimeters are very different and fluctuations in the energy sharing between them have a big effect. Given the fine longitudinal segmentation of both calorimeters, an extension of the weighting technique used in [2], could have been applied to reduce the effects of the different  $r_e/\pi$  ratios of the two calorimeters and thus obtain the best energy resolution.

### 3.4 Longitudinal Shower Distributions

For the optimization of the length of a hadron calorimeter, longitudinal shower distributions have to be known. They are shown in Fig. 8 for the hadronic calorimeter for energies from 5 to 210 GeV for all events, and in Fig. 9 for the events with the interaction vertex in the first module ( $\sim 0.45$  interaction lengths). The curves are normalized, so that their integrals give the incident energy. The horizontal axes are nominal interaction lengths  $\lambda_{INT}$  as given in the Particle Data Group tables. The corresponding cumulative distributions are shown in Fig. 10 and Fig. 11. It should be noted that only the first 5.4 interaction lengths contain uranium as absorber, the rest consisting of iron.

The data have been fitted by a phenomenological function, which allows extrapolation to other energies than the measured ones. For the energy deposit  $dE/dx$  as a function of the distance  $x$  from the shower vertex, we use the following parametrization:

$$\frac{dE}{dx}(x) = E \left\{ \alpha \frac{b^{a+1}}{\Gamma(a+1)} x^a \exp(-bx) + (1-\alpha) c \exp(-cx) \right\} \quad (9)$$

The second term describes the exponential dependence, obvious from Fig. 9 for large distances from the shower vertex. The first term, which has the shape used to parametrize electromagnetic showers [14], describes the electromagnetic energy close to the shower vertex. Given the readout segmentation of  $0.45 \lambda_{INT}$  and  $13.5 X_0$ , coarse on the scale of electromagnetic shower development, the description of the data is not very sensitive to the exact values of the parameters  $a$  and  $b$ . We have chosen values [14] which describe electromagnetic showers in uranium at 20 GeV:

$$\begin{aligned} a &= 3 \\ b [\lambda_{INT}^{-1}] &= 19.5 \end{aligned}$$

The remaining parameters have been determined by fitting equation (9) to the measurements. Above 5 GeV reasonable fits, as shown by the solid lines in Fig. 8, have been obtained for:

$$\begin{aligned} \alpha &= 0.13 \pm 0.02 \\ c [\lambda_{INT}^{-1}] &= (0.67 \pm 0.03) - (0.166 \pm 0.003) \ln \frac{E [\text{GeV}]}{50} \end{aligned}$$

The chosen parametrization minimizes correlations between the errors of the parameters. The shower distributions measured from the front end of the calorimeter ( $t$ ) for particles without selection of shower vertices are given by the convolution of  $dE/dx(x)$  with the shower vertices:

$$\frac{dE}{dt} = \frac{1}{\lambda_\pi} \int_0^t \exp\left(-\frac{x}{\lambda_\pi}\right) \frac{dE}{dx}(t-x) dx \quad (10)$$

where  $\lambda_\pi = 1.11$  is the interaction length of the incoming hadrons in units of the nominal interaction length as given in the Particle Data Group tables<sup>2</sup>. The curves in Fig. 8 are obtained from equation (10) using the parameters determined above.

For the determination of the optimum length of a calorimeter, the fraction of events with a certain shower leakage has to be known. The fraction of events which have 95% containment in the hadronic calorimeter as a function of the calorimeter length in units of  $\lambda_{INT}$  can be obtained from Fig. 12 and Fig. 13. These distributions have been used to define the length of the uranium calorimeter of the ZEUS detector for the HERA accelerator. More details can be found in [15].

## 4 Conclusions

From the measurement of the response to hadrons, electrons and muons in the energy range between 5 and 210 GeV in a sampling calorimeter with 10 mm uranium plates and 5 mm plastic scintillator we find:

<sup>2</sup>One module of the hadronic calorimeter corresponds to 45 % of an interaction length for protons and 37 % for pions.

- the response of electrons relative to hadrons " $e/\pi$ " is about 0.8 independent of the incident energy for 75 ns integration time, increasing for shorter integration times.
- the sampling fractions of electrons divided by the sampling fraction of minimum ionizing particles " $e/mip$ " is about 0.6.
- an electromagnetic calorimeter with 1.57 mm uranium plates and 4 mm plastic scintillator in front of the above calorimeter does not improve the hadronic energy resolution.
- the longitudinal shower development and criteria for containment to optimize the length of actual calorimeters are given.

Together with data from other experiments [2,3,6,7,8], our data confirm that the relative response of electrons to hadrons can be tuned in a uranium scintillator calorimeter by varying the thickness of absorber and detection material.

## Acknowledgement

We are grateful for the hospitality at CERN, where the measurements have been done. We should like to thank D. Plane and his colleagues from the CERN-EA group for preparing and setting up the beam line and for the beam calculations. Part of this work has been supported by the Bundesministerium für Forschung und Technologie, Bonn.

## References

- [1] **ZEUS Collaboration**; *The ZEUS Detector, Technical Proposal*; March 1986
- [2] **DE VINCENZI, M. et al.**; Nucl. Inst. Meth. **A243** (1986) 348
- [3] **DE VINCENZI, M. et al.**; Nucl. Inst. Meth. **A248** (1986) 326
- [4] **PETERS, J. H.**; *Untersuchungen an einem Uran Scintillator Kalorimeter mit Elektronen und Hadronen*; DESY F14/86-03 (1986)
- [5] **ZEUS-CALORIMETER GROUP**; *Test of a Uranium Scintillator Calorimeter*; to be published
- [6] **BOTNER, O. et al.**; Phys. Scripta **23** (1981) 556
- [7] **ANDERS, B. et al.**; *Performance of a Uranium Scintillator Calorimeter*; DESY 86-105 (1986)
- [8] **WIGMANS, R.**; *NA34 U-Scintillator Calorimeter and Radiation Damage Studies*; in: Proc. of WORKSHOP ON COMPENSATED CALORIMETRY, Pasadena; CALT-68-1305 (1985)
- [9] **FABJAN, C. W.**; *Calorimetry in High-Energy Physics*; CERN-EP/85-54 (1985)
- [10] **WIGMANS, R.**; *On the Energy Resolution of Uranium and other Hadron Calorimeters*; CERN-EP/86-141 (1986)
- [11] **BRÜCKMANN, H. et al.**; *Hadron Calorimetry: A Puzzle of Physics*; DESY 86-155 (1986)  
**LEROY C. et al.**; Nucl. Inst. and Meth. **A252** (1986) 4
- [12] **GENNIS, M.**; *Entwurf und Test eines Elektromagnetischen Kalorimeters*; Diploma Thesis, Universität Hamburg (1987)
- [13] **STERNHEIMER, R. M. et al.**; Phys. Rev. **B3** (1971) 3681  
**STERNHEIMER, R. M. et al.**;  
Atomic Data and Nuclear Data Tables **30** (1984) 261  
**LOHMANN, W. et al.**; *Energy Loss of Muons in the Energy Range 1-10000 GeV*; CERN 85-54 (1985)
- [14] **AMALDI, U.**; Phys. Scripta **23** (1981) 409
- [15] **KRÜGER, J.**; *Shower Development in an Uranium/ Scintillator Calorimeter (WA 78) and the Requirements for the Hadron Calorimeter of the ZEUS Detector*; ZEUS-Note 86-019 (1986)

## Table Captions

- Tab. 1 : Layer structure of the calorimeters
- Tab. 2 : Particle content of the beam, the hadrons are mainly pions
- Tab. 3 : Response of the electromagnetic (EM) and the hadronic calorimeter (HAD) for different particles. Given are the mean pulse heights (PH) in ADC channel numbers, the standard deviations  $\sigma_E$  of the measured electron and hadron distribution, and for the HAD-calorimeter the uncorrected response ratio  $e/\pi$ . The contribution of the beam spread to  $\sigma_E$  has not been subtracted.
- Tab. 4 : The electron sampling fraction "e" for the EM- and the HAD-calorimeter determined with the two different methods described in the text.  $dE/dx(\mu)|_{SCI}$  is the specific energy loss in the scintillator due to ionization, bremsstrahlung and pair production obtained by interpolating the values given in [13].  $\Delta E(\mu)|_{SCI}$  is the corresponding energy loss for the entire calorimeters.
- Tab. 5 : Material densities and the specific energy loss of a hypothetical minimum ionizing particle "mip" in the different materials of the calorimeters and the "e/mip" ratios of the EM- and the uranium part of the HAD-calorimeter.

## Figure Captions

- Fig. 1 : Schematic layout of the experimental set-up.
- Fig. 2 : Response of the hadronic calorimeter (HAD) to 30 GeV hadrons, electrons and muons. The curves are Gaussian functions for hadrons and electrons and a Landau curve convoluted by a Gaussian for the muons.
- Fig. 3 : Response of the HAD-calorimeter to hadrons and electrons for different energies. The data are normalized to the number of entries of each distribution. The curves are Gaussian fits to the data, which give the mean values and standard deviations listed in Tab. 3.
- Fig. 4 : Ratio of electron to hadron response for different scintillator sampling calorimeters. The references of the different measurements are given in square brackets. For the detailed configuration (e.g. A,B,U5 ...) see references.
- Fig. 5 : Ratio of electron to hadron response for the HAD-calorimeter at 30 GeV as a function of the ADC integration time. In the measurement, the gate preceded the pulse by about 15 ns which reduces the effective gate length.
- Fig. 6 : Muon response at 30 GeV in the electromagnetic calorimeter (EM). The curve is a fit of a Landau function convoluted with a Gaussian.
- Fig. 7 : Energy resolution for 30 GeV electrons and hadrons for the combined set-up of EM- and HAD-calorimeters as a function of the intercalibration constant  $\alpha$ .
- Fig. 8 : Longitudinal energy deposition in the HAD-calorimeter for hadrons between 5 and 210 GeV. The curves are normalized to an area equal to the incident energy. The horizontal scale is the calorimeter depth in nominal interaction lengths. The transition between the uranium and iron section of the HAD-calorimeter occurs at  $5.4 \lambda_{INT}$ . The curves are the phenomenological shower parametrizations described in the text.
- Fig. 9 : Similar to Fig. 8 but for events with shower vertices in the first module of the calorimeter. The shower vertex is selected via a pulse height cut of more than  $n$  minimum ionizing particles. ( $n = 4$  for 5 - 40 GeV,  $n = 8$  for 135 and 210 GeV).
- Fig. 10 : Integral energy deposition. The fraction of energy in % deposited beyond a given calorimeter depth in units of  $\lambda_{INT}$  is given.
- Fig. 11 : Integral energy deposition for events interacting in the first  $0.45 \lambda_{INT}$  of the calorimeter. The fraction of energy in % deposited beyond a given calorimeter depth in units of  $\lambda_{INT}$  is given.
- Fig. 12 : Fraction of events with 95% energy containment as a function of the calorimeter depth for hadrons.
- Fig. 13 : Identical to Fig. 12 but for hadrons interacting in the first calorimeter module. These distributions correspond approximately to the containment of jets (more details can be found in [15]).

## Tables

Table 1: Layer Structure of the Calorimeters

	EM-Calorimeter	HAD-Calorimeter	
		Uranium Part	Iron Part
sampling layer	0.5 mm Fe	1 mm Fe	25 mm Fe
	1.57 mm U	10 mm U	5 mm NE 110
	0.5 mm Fe	1 mm Fe	
	4.0 mm SCSN 38	5 mm NE 110	
readout layer	4.0 mm Al	4 sampling layers	4 sampling layers
	4.0 mm SCSN 38		
	8 sampling layers		
	4.0 mm Al		
total calorimeter	6 readout layers	12 readout layers	13 readout layers

Table 2: Particle Content of Beam

Energy [GeV]	Fraction [%]		
	Electrons	Muons	Hadrons
5.1	52.6	3.5	43.9
10.1	22.4	3.7	73.9
20.2	7.2	3.9	88.9
30.3	4.5	4.3	91.2
40.3	2.7	3.5	93.8

Table 3: Response to Different Particles

Energy [GeV]	EM-Calorimeter			HAD-Calorimeter					
	PH( $\mu$ ) [ch]	PH(e) [ch]	$\frac{\sigma_E}{E}(e)$ [%]	PH( $\mu$ ) [ch]	PH(e) [ch]	$\frac{\sigma_E}{E}(e)$ [%]	PH( $\pi$ ) [ch]	$\frac{\sigma_E}{E}(\pi)$ [%]	e/ $\pi$
5.1	56	576	12.2	79.2	176	18.2	226	23.7	0.78
10.1	53	1200	10.0	80.4	337	12.5	414	17.5	0.81
20.2	-	-	-	81.5	639	9.7	780	13.7	0.82
30.3	55	3300	6.7	84.1	955	8.4	1163	12.1	0.82
40.3	56	4415	6.3	86.5	1263	7.7	1533	11.2	0.82

Table 4: Electron Sampling Fraction

Energy [GeV]	$\frac{dE}{dz}(\mu)_{SCI}$ [ $\frac{MeVcm^2}{g}$ ]	EM-Calorimeter			HAD-Calorimeter: Uranium Part		
		$\Delta E(\mu)_{SCI}^{meth.1}$ [MeV]	e [%]		$\Delta E(\mu)_{SCI}^{meth.1}$ [MeV]	e [%]	
			Meth.1	Meth.2		Meth.1	Meth.2
5.1	2.30	52.7	10.6	10.7	57.0	2.48	2.48
10.1	2.41	55.2	12.4	12.8	59.7	2.48	2.56
20.2	2.51	57.5	-	-	62.2	2.41	2.59
30.3	2.58	59.1	11.6	12.8	63.9	2.39	2.67
40.3	2.63	60.2	11.7	13.4	65.1	2.37	2.75
Mean			11.6	12.4		2.43	2.61

Table 5: Materials in Calorimeter and Energy Loss for Minimum Ionizing Particle (mip)

Material	Density [ $\frac{g}{cm^3}$ ]	Energy Loss mip [ $\frac{MeVcm^2}{g}$ ]	Total Thickness [cm]	
			EM-Calorimeter	HAD-Calorimeter Uranium Part
Aluminium	2.70	1.62	4.8	-
Uranium	18.50	1.09	7.5	48.0
Iron	7.87	1.48	4.8	9.6
SCSN 38	1.06	1.95	21.6	-
NE 110	1.032	1.95	-	24.0
Average e/mip		Method 1	0.71	0.57
Average e/mip		Method 2	0.76	0.61

# Figures

- |           |                             |       |                      |
|-----------|-----------------------------|-------|----------------------|
| $\hat{C}$ | Cerenkov Counter            | $B_1$ | Beam Trigger 1       |
| A         | Anticounter                 | $B_2$ | Beam Trigger 2       |
| F         | Finger Hodoscope            | $H_1$ | Veto Wall 1          |
| AC        | Albedo Counter              | $H_2$ | Veto Wall 2          |
| EM        | Electromagnetic Calorimeter | HAD   | Hadronic Calorimeter |

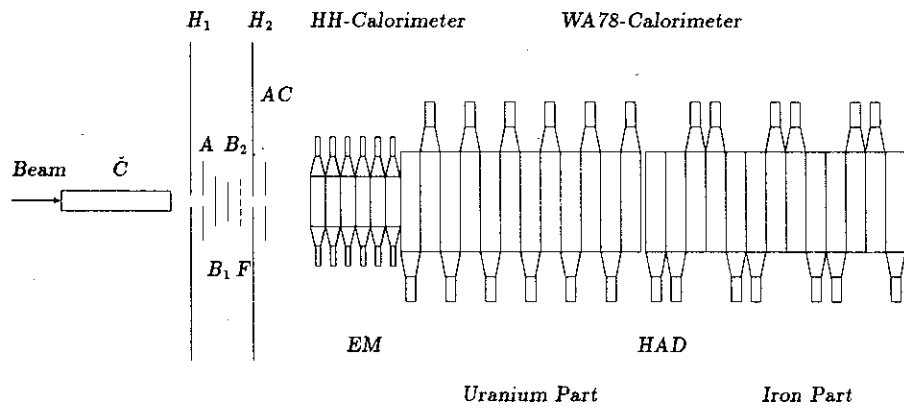


Figure 1: Experimental Set-Up

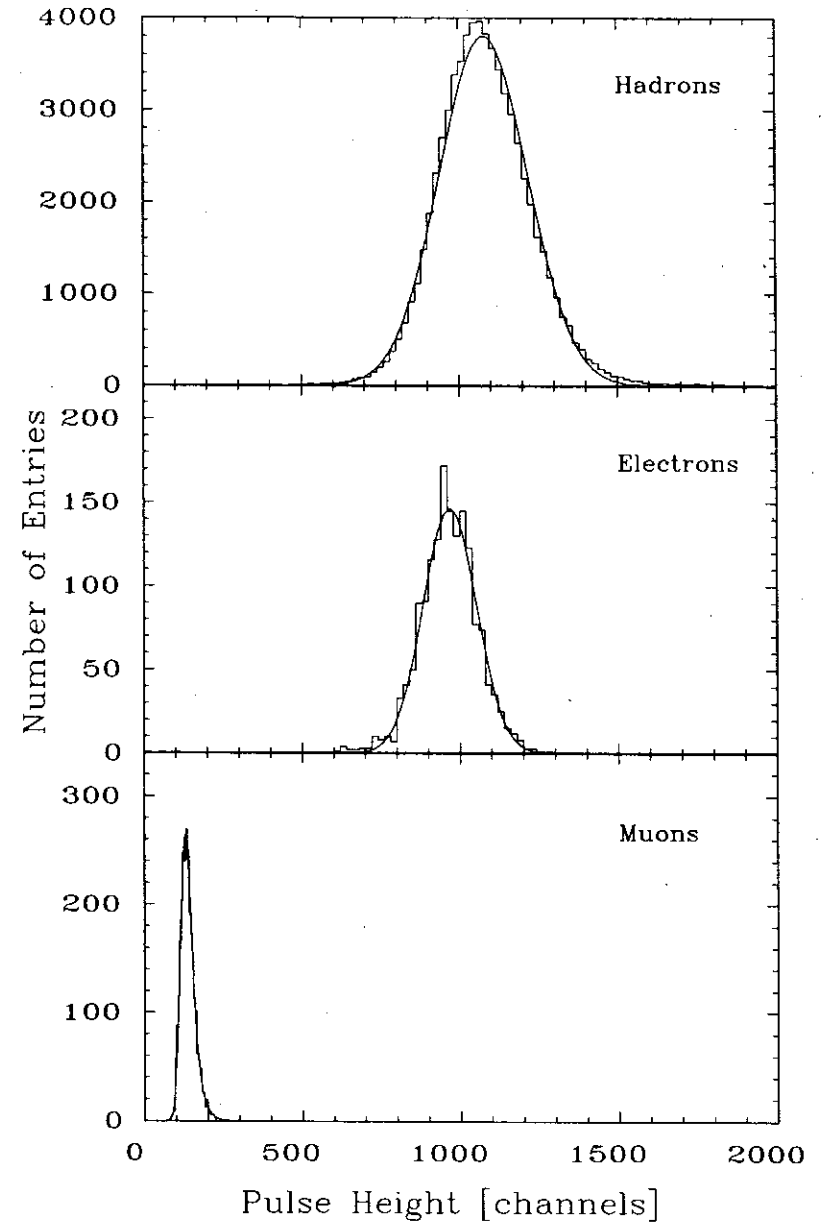


Figure 2: Hadron, Electron and Muon Response in the HAD Calorimeter at 30 GeV

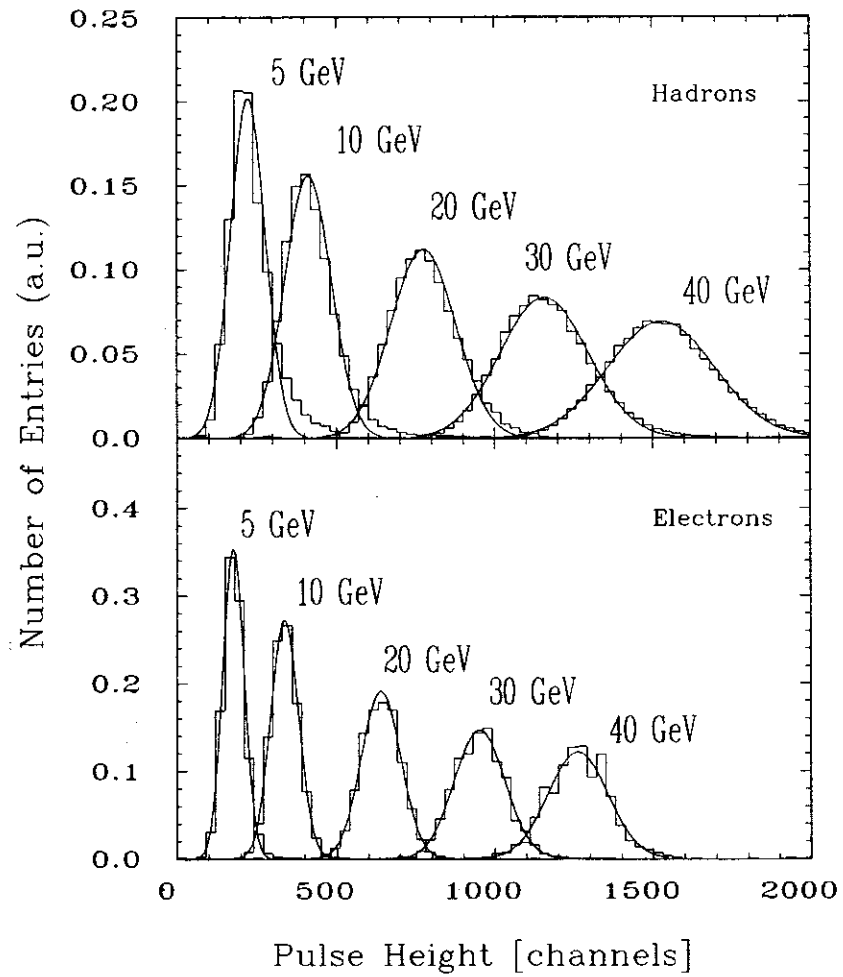


Figure 3: Hadron and Electron Response of the HAD-Calorimeter for Various Beam Energies

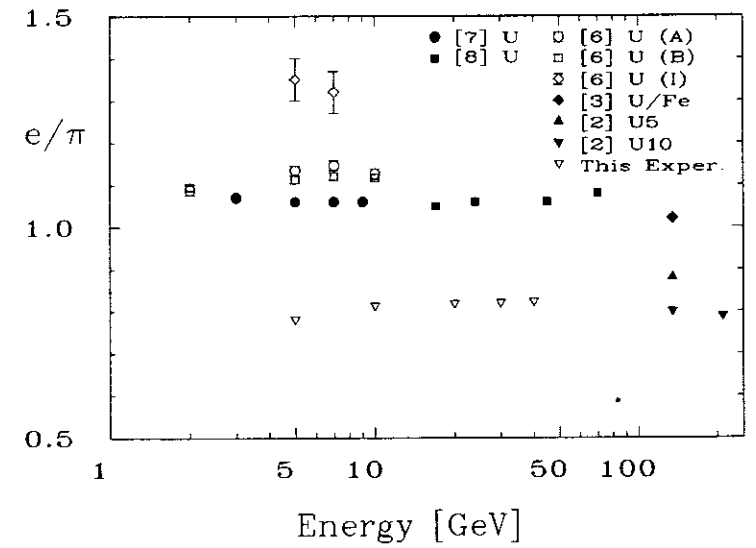


Figure 4:  $e/\pi$ -Ratio for Different Hadron Calorimeters

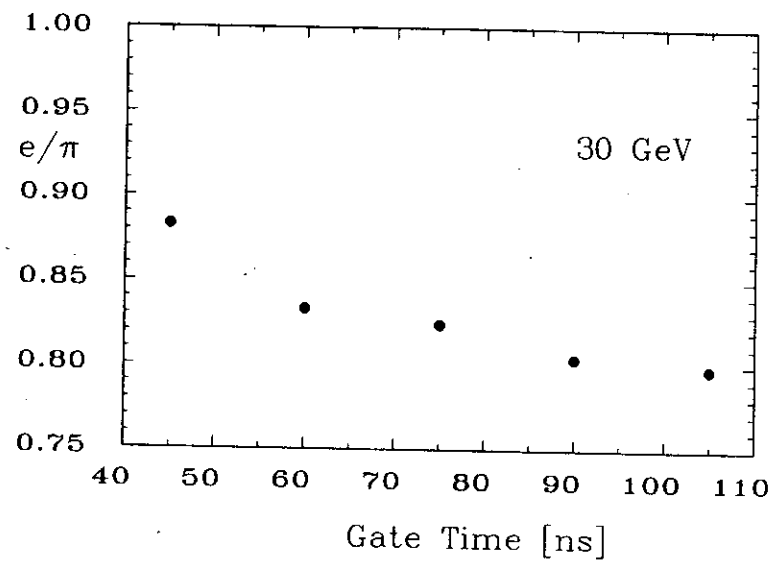


Figure 5:  $e/\pi$ -Ratio at 30 GeV as a Function of the ADC Gating Time

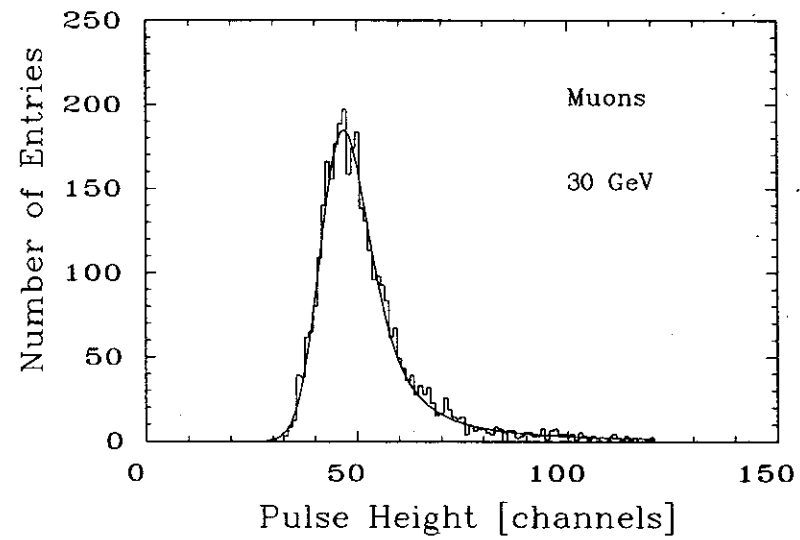


Figure 6: Muon Response at 30 GeV in the Electromagnetic Calorimeter

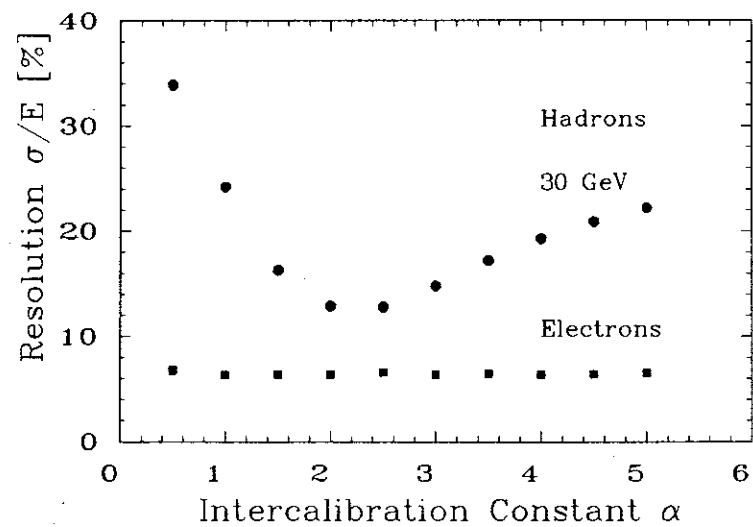


Figure 7: Energy Resolution of the Combined Electromagnetic and Hadronic Calorimeter as a Function of the Relative Calibration Constant  $\alpha$

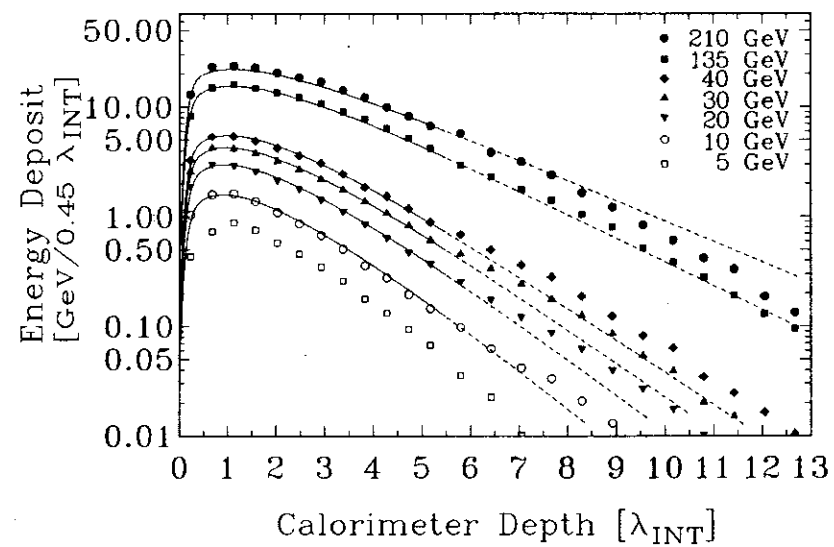


Figure 8: Longitudinal Energy Deposition for Beam Momentum of 5 to 210 GeV for all Events

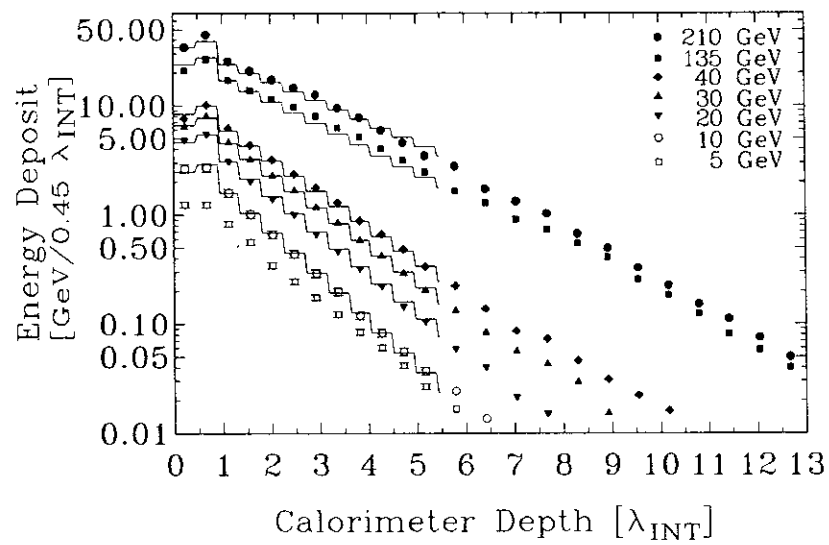


Figure 9: Longitudinal Energy Deposition for Beam Momentum of 5 to 210 GeV for Events with Shower Vertices in the First Module

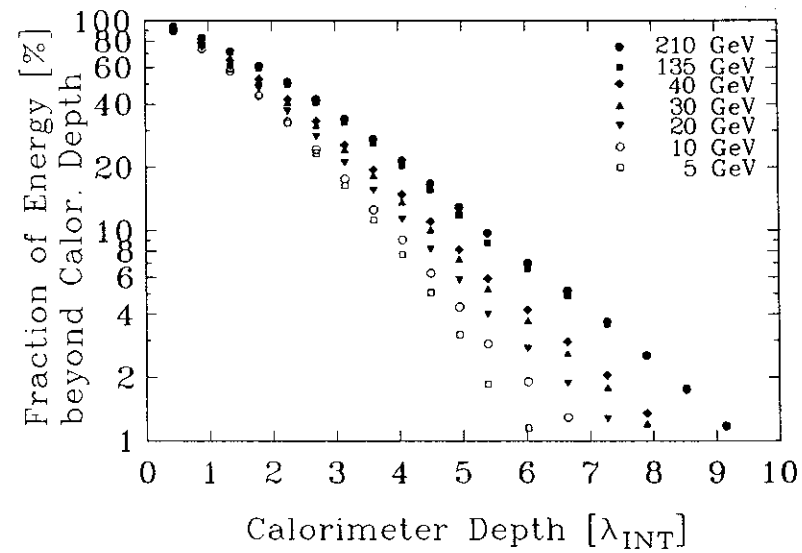


Figure 10: Cumulative Distributions of Longitudinal Energy Deposition for all Events

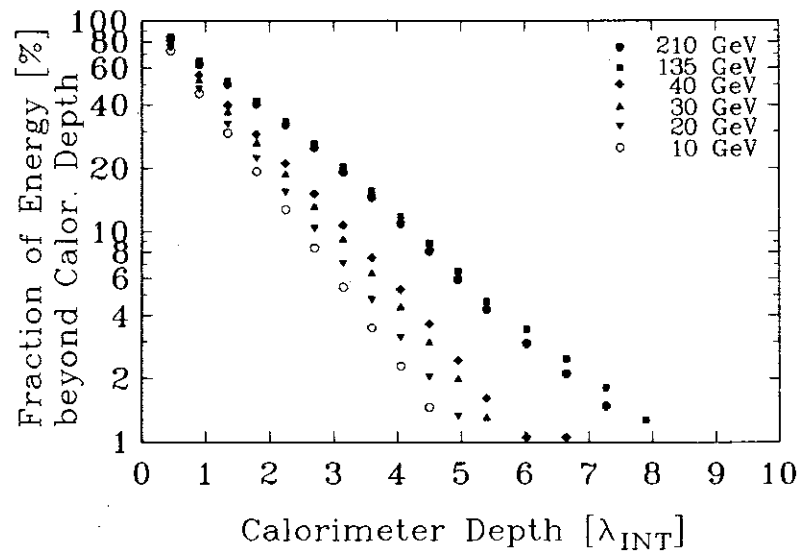


Figure 11: Cumulative Distributions of Longitudinal Energy Deposition for Events with Shower Vertices in the First Module

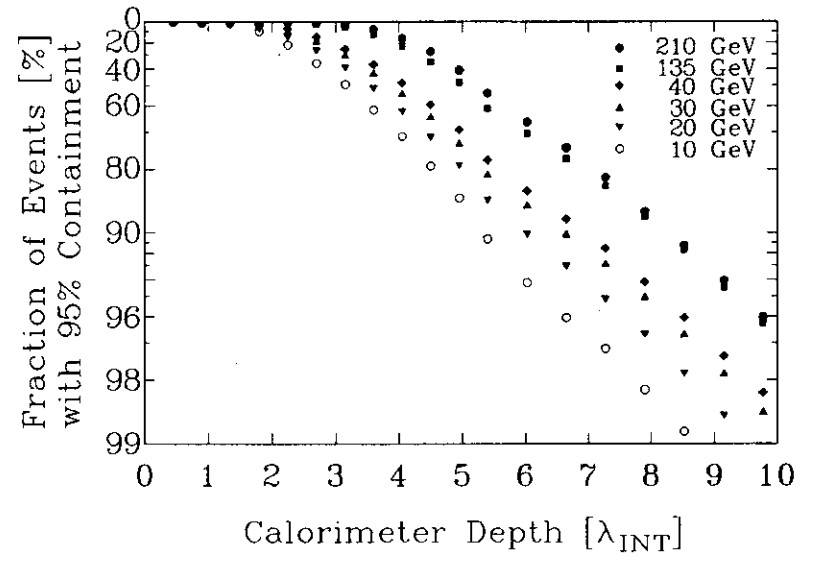


Figure 12: Fraction of Events with 95 % Containment in the Calorimeter for all Events

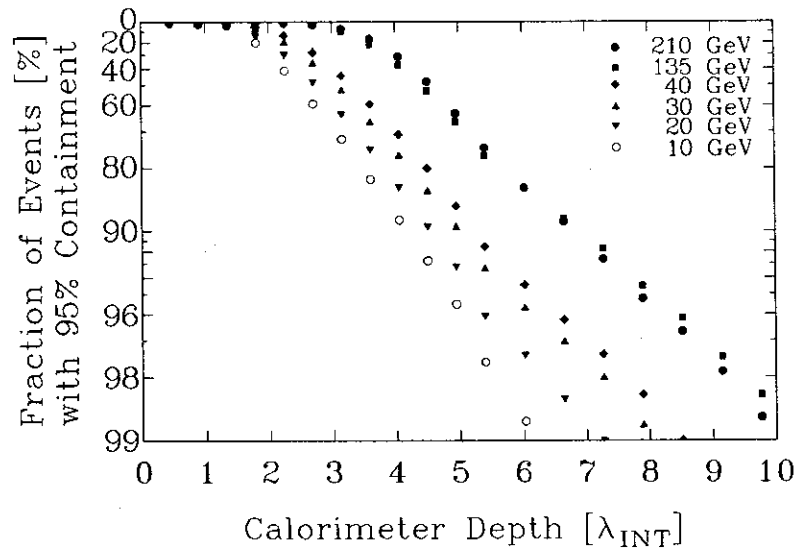


Figure 13: Fraction of Events with 95 % Containment in Calorimeter for Events with Shower Vertices in the First Module